Nanoscale Research Letters
a SpringerOpen Journal

NANO EXPRESS Open Access

Size dependence of the magnetic properties of Ni nanoparticles prepared by thermal decomposition method

Xuemin He[1], Wei Zhong[1*], Chak-Tong Au[2] and Youwei Du[1]

Abstract

By means of thermal decomposition, we prepared single-phase spherical Ni nanoparticles (23 to 114 nm in diameter) that are face-centered cubic in structure. The magnetic properties of the Ni nanoparticles were experimentally as well as theoretically investigated as a function of particle size. By means of thermogravimetric/differential thermal analysis, the Curie temperature T_C of the 23-, 45-, 80-, and 114-nm Ni particles was found to be 335°C, 346°C, 351°C, and 354°C, respectively. Based on the size-and-shape dependence model of cohesive energy, a theoretical model is proposed to explain the size dependence of T_C. The measurement of magnetic hysteresis loop reveals that the saturation magnetization M_S and remanent magnetization increase and the coercivity decreases monotonously with increasing particle size, indicating a distinct size effect. By adopting a simplified theoretical model, we obtained M_S values that are in good agreement with the experimental ones. Furthermore, with increase of surface-to-volume ratio of Ni nanoparticles due to decrease of particle size, there is increase of the percentage of magnetically inactive layer.

Keywords: Size dependence; Curie temperature; Cohesive energy; Magnetically inactive layer

Background

The transition metal nickel shows distinct magnetic and catalytic properties [1,2]. In nanostructure, Ni has great application potential in fields such as pharmaceutical synthesis [3], magnetic biocatalysis [4], biomolecular separation [5], and biosensor [6]. In the literatures, there are reports on the preparation and properties of novel Ni nanomaterials such as sea urchin-like Ni nanoparticles [7], tetragonal Ni nanoparticles [8], hexagonal close-packed (*hcp*) Ni nanoparticles [9], conical Ni nanorods [10], triangular and hexagonal Ni nanosheets [11], and Ni nanochains [12]. It is known that the performance of technological devices is greatly influenced by the purity, structure, shape, and size of Ni nanoparticles. Hence, it is of great significance to prepare high-quality Ni nanomaterials of specificity using convenient and low-cost methods.

For the fabrication of Ni nanoparticles, methods such as sputtering [13,14], solution glow discharge [15], pulsed laser ablation [6], reversed micelles [16], thermal decomposition [17-20], and wet chemical reduction [7,21,22] are used. Among them, the ones based on thermal decomposition are preferred. The single-step process is facile, environment-benign, inexpensive, and reproducible, yielding high-quality Ni powders that can be controlled in terms of structure, morphology, size, and size distribution. It should be pointed out that pure Ni nanoparticles are difficult to prepare because they are easily oxidized. One of the ways to evade the formation of oxide or hydroxide is to carry out the pyrolysis process in organic media. For example, relatively large Ni nanoparticles were prepared through thermal decomposition of $Ni(ac)_2\ 4H_2O$ in oleylamine in the presence of 1-adamantane carboxylic acid (ACA) and trioctylphosphine oxide (TOPO) [19]. Furthermore, structure-controlled Ni nanoparticles were prepared via thermal decomposition of $Ni(ac)_2\ 4H_2O$ in long-chain amines that acted both as solvent and reducing agent [23]. More interestingly, trigonal Ni nanoparticles were prepared by reacting $Ni(COD)_2$ in tetrahydrofuran with tetra-

* Correspondence: wzhong@nju.edu.cn
[1]National Laboratory of Solid State Microstructures and Jiangsu Provincial Laboratory for NanoTechnology, Department of Physics, Nanjing University, Nanjing 210093, China
Full list of author information is available at the end of the article

n-octylammonium carboxylates (as reductant and stabilizer) [24]. Despite the synthesis of superior Ni nanomaterials through the pyrolysis of organometallic salts in organic media has been known for quite some time, the synthesis of Ni nanoparticles 20 to 100 nm in size has only been reported lately.

Bulk Ni exhibits a rock-salt structure and is ferromagnetic (Curie temperature of bulk Ni T_{Cb} = 358°C) and electroconductive [25]. In contrast to the bulk counterparts, Ni nanoparticles show magnetic parameters (such as Curie temperature T_C, saturation magnetization M_S, and coercivity H_C) that vary with particle size, usually in a non-linear fashion. Despite the endless number of reports on magnetic studies of Ni nanoparticles [1,10,18,26-30], the influence of particle size on the magnetic properties has not been systematically studied. It is envisaged that the application of Ni nanoparticles can be widened once the intrigue relationship between magnetic properties and particle size of Ni nanomaterials can be delineated.

Herein, we report a facile and reproducible process for large-scale synthesis of face-centered cubic (*fcc*) Ni nanoparticles (spherical and 23 to 114 nm in diameter). We controlled the size of Ni nanoparticles by regulating the synthesis temperature. We studied the influence of particle size on Curie temperature, saturation magnetization, and coercivity. We establish the size dependence of magnetic properties based on experimental as well as theoretical results, and comment on the critical size of Ni nanoparticles and percentage of magnetically inactive layer.

Methods

Spherical Ni nanoparticles were prepared through high-temperature reductive decomposition of nickel(II) acetylacetonate ([Ni(acac)$_2$]) with oleic acid (OA) and oleylamine (OAm) both as surfactant and solvent. In a typical synthesis process, [Ni(acac)$_2$] (0.51 g, 2 mmol), OA (12 mL, 38 mmol), and OAm (18 mL, 55 mmol) were mixed and stirred in a three-necked flask. The mixture was heated at 130°C in H-320 conduction oil for 30 min under an argon atmosphere to give a clear emerald solution. Under the Ar blanket, the solution was heated to 240°C and kept at this temperature for 1 h. Then, the solution was cooled down to room temperature to obtain a black colloidal solution. A black precipitate was separated upon the addition of ethanol and hexane followed by centrifugation. The black substance was washed using a mixture of ethanol and toluene, and vacuum dried in an oven at 60°C overnight. Under similar reaction conditions, the size of the spherical Ni nanoparticles was tuned from 23 to 114 nm by simply increasing the reaction temperature from 240°C to 285°C as shown in Table 1.

X-ray diffraction (XRD) patterns of all the samples were obtained by using an X-ray diffractometer (Philips X'pert, Philips, Amsterdam, The Netherlands) with Cu Kα radiation. To examine the morphology and particle sizes, a field-emission scanning electron microscope (SEM) (Hitachi S-4800, Hitachi Ltd., Chiyoda-ku, Japan) was used. High-resolution transmission electron microscope (TEM) image and selected-area electron diffraction (SAED) pattern were obtained from a FEI Tecnai G2-F30 instrument (FEI, Hillsboro, OR, USA) operated at accelerating voltage of 300 kV. In the TEM experiment, the incident electron beam was along the direction perpendicular to the sample. The sample was transferred onto a copper grid by solution dripping with the sample powder under sonication in ethanol. The Curie temperature was measured using a thermogravimetric (TG)/differential thermal analysis (DTA) instrument (Scinco STA-1500, Scinco Co. Ltd., Seoul, South Korea) equipped with a piece of $Nd_2Fe_{14}B$ permanent magnet during sample heating (up to 500°C) in argon at a rate of 10°C/min. For comparing, the TG/DTA measurement of a bulk Ni sample (nickel sphere) was conducted under the same conditions. Magnetic measurements were carried out with a vibrating sample magnetometer (VSM) (Lake Shore 7300, Lake Shore Cryotronics, Inc., Westerville, OH, USA). The hysteresis was recorded for powder samples in gelatin capsule, and the hysteresis loops were obtained in a magnetic field up to ±10 kOe. Magnetization versus temperature (*M-T*) curves were measured in the range 30°C to 400°C using an applied magnetic field of 5 kOe.

Results and discussion

Figure 1a shows the powder XRD patterns of the Ni nanoparticle samples synthesized at 240°C, 255°C, 270°C, and 285°C. All samples are single-phase with face-centered cubic (*fcc*) structure, and no phase of NiO or other impurity is observed. The three obvious peaks (2θ = 44.58°, 51.90°, 76.54°) can be assigned to the (111), (200), and (220)

Table 1 Size and magnetic parameters for the Ni-particle samples obtained at different temperatures

Sample	T (°C)	D (nm)	T_C (°C)	M_S (emu/g)	M_r (emu/g)	H_C (Oe)	t/D (%)
a	240	23	335	40.47	6.81	156	4.26
b	255	45	346	44.33	9.67	119	3.09
c	270	80	351	46.47	12.56	76	2.43
d	285	114	354	47.80	17.59	17	2.03

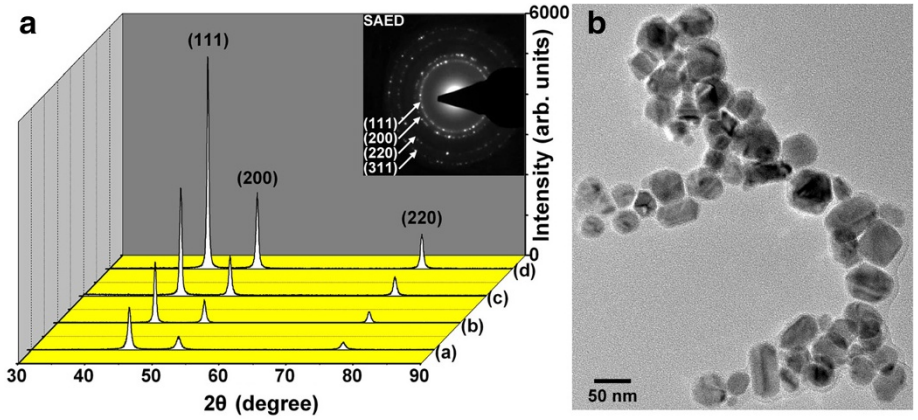

Figure 1 XRD patterns (a) and HRTEM image (b). Ni nanoparticles formed at (a) 240°C, (b) 255°C, (c) 270°C, and (d) 285°C. SAED pattern and HRTEM image relative to Ni nanoparticles formed at 255°C.

planes of Ni crystal lattice, respectively. It is clear that there is peak broadening upon decrease of reaction temperature. In other words, the particle size of the prepared Ni nanoparticles increases with increasing reaction temperature, and this is confirmed in SEM analysis (show later). As can be seen in the SAED pattern (inset of Figure 1a), perfect cubic symmetry can be clearly identified for the polycrystalline Ni nanoparticles. The high-resolution TEM image in Figure 1b presents the granular morphology and further reveals the surface nature of magnetically dead layer.

Figure 2 shows the representative SEM images of the Ni nanoparticles formed at 240°C, 255°C, 270°C, and 285°C. It is observed that most Ni particles are oval or spherical in shape. The particle-size analysis based on SEM images shows normal Gaussian distributions (Figure 3). It is apparent that the mean particle size increases with increasing reaction temperature, in excellent agreement with the results of XRD analysis. Hereinafter, D denotes the mean particle sizes which are 23, 45, 80, and 114 nm for the samples formed at 240°C, 255°C, 270°C, and 285°C, respectively, and the symbol 'Δ' denotes the absolute deviation obtained from the Gaussian fitting. It can be seen that the absolute deviation increases with the increase of mean particle size. It is reasonable to deduce that the change of reaction temperature will result in density difference of organic functional groups on the particle surface [31]. We propose that the control of reaction temperature is a mean for easy regulation of particle size and size distribution during the growth process.

The TG/DTA curves were obtained with the samples kept under an argon atmosphere. In order to obtain information of Curie temperature, a piece of $Nd_2Fe_{14}B$ permanent magnet was placed on top of the furnace chamber during the test. Usually, the magnetization per unit mass (or unit volume) decreases with increasing temperature. When the temperature reaches the Curie temperature of material, magnetization becomes zero and ferromagnetism disappears [32]. At that moment, there is no attraction between the magnet and the sample. As a result, the relative weight close to the Curie temperature will become larger. In the TG curves of Figure 4a,b,c,d, the relative weight decreases slowly at first and reaches a minimum at temperature T_1, then increases quickly and reaches a maximum at temperature T_2, and shows a gentle decline with further rise of temperature. The DTA curves in Figure 4a, b,c,d show a phase-transition peak between T_1 and T_2, and the phase-transition temperature is exactly the Curie temperature T_C. For the Ni nanoparticles with particle sizes of 23, 45, 80, and 114 nm, the T_C values are 335°C, 346°C, 351°C, and 354°C, respectively. For comparison, the TG/DTA curve of a bulk Ni sample is shown in Figure 4e. Obviously, the T_C values of these Ni nanoparticles are lower than that of bulk nickel (358°C).

The T_C value decreases with the decrease of particle size (see the solid circles in Figure 5), showing a strong size effect. In theory, the cohesive energy E_n of free-standing nanoparticles with random shape can be described as [33]

$$E_n = E_b\left(1-\frac{6\mu}{n^{1/3}C^{2/3}\pi k^2}\right), \quad (1)$$

where E_b denotes the cohesive energy of the corresponding bulk materials, μ is the shape factor, n is the atomic number of nanocrystals, C is the atomic number of the structure cell, and k is the ratio between equivalent atomic radius and lattice parameter. Considering that the Curie temperature is proportional to the cohesive energy [34], it is reasonable to express the Curie

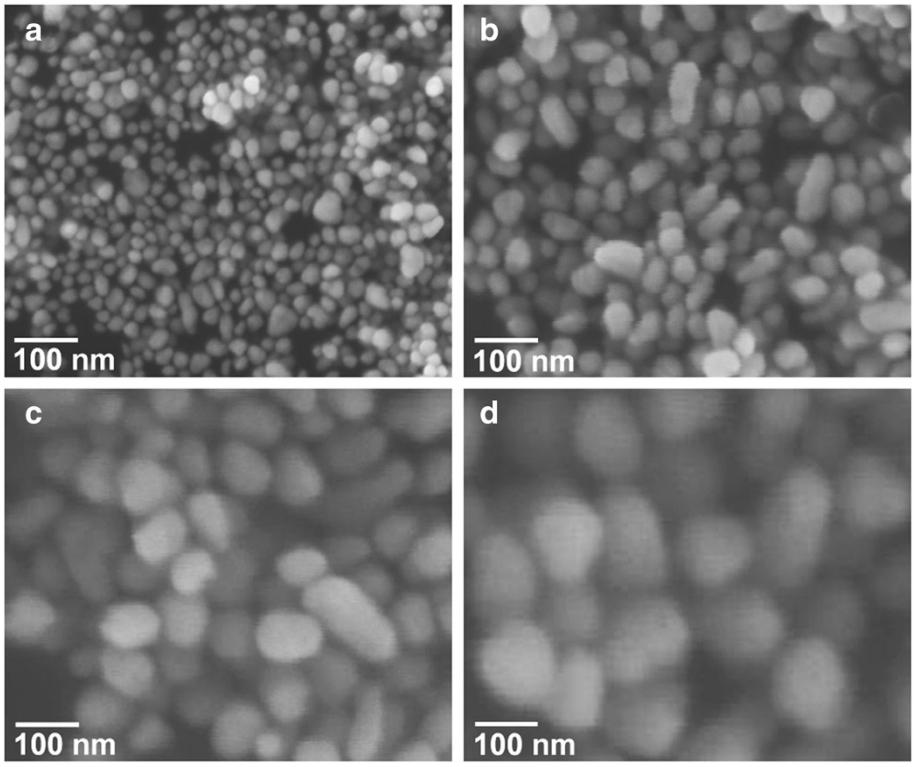

Figure 2 SEM images. Ni nanoparticles formed at **(a)** 240°C, **(b)** 255°C, **(c)** 270°C, and **(d)** 285°C.

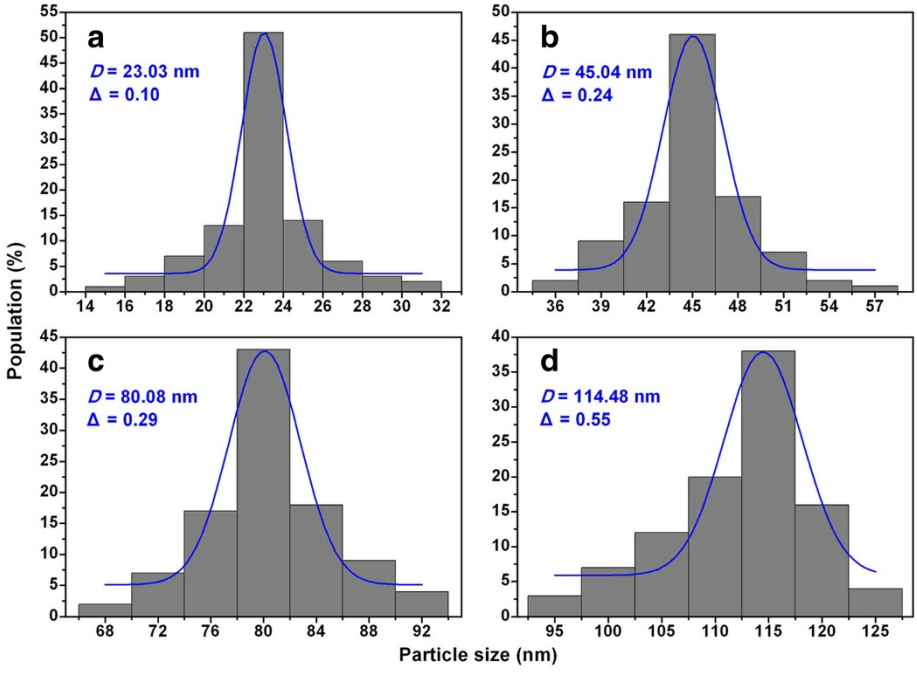

Figure 3 Size distribution histograms. Ni nanoparticles formed at **(a)** 240°C, **(b)** 255°C, **(c)** 270°C, and **(d)** 285°C. The blue lines represent the results of Gaussian fitting.

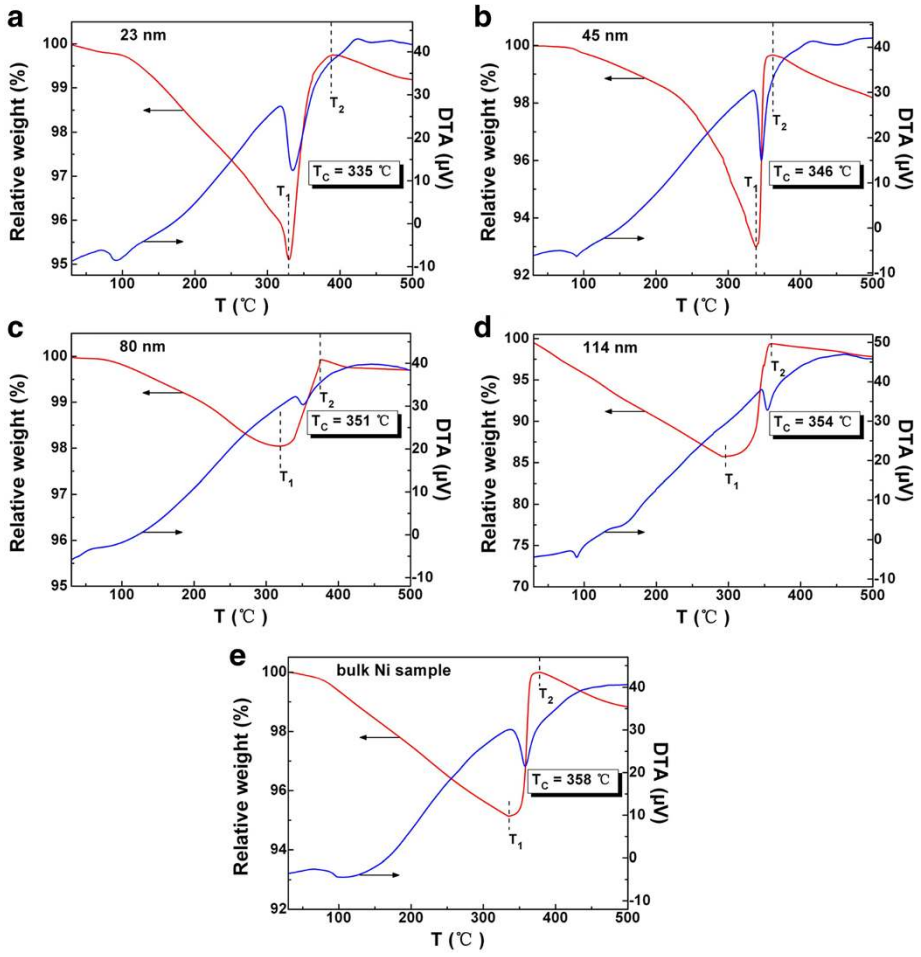

Figure 4 TG/DTA curves. Ni nanoparticles with particle sizes of **(a)** 23, **(b)** 45, **(c)** 80, **(d)** 114 nm, and **(e)** the corresponding bulk Ni sample, obtained in the presence of a piece of $Nd_2Fe_{14}B$ permanent magnet and under argon atmosphere.

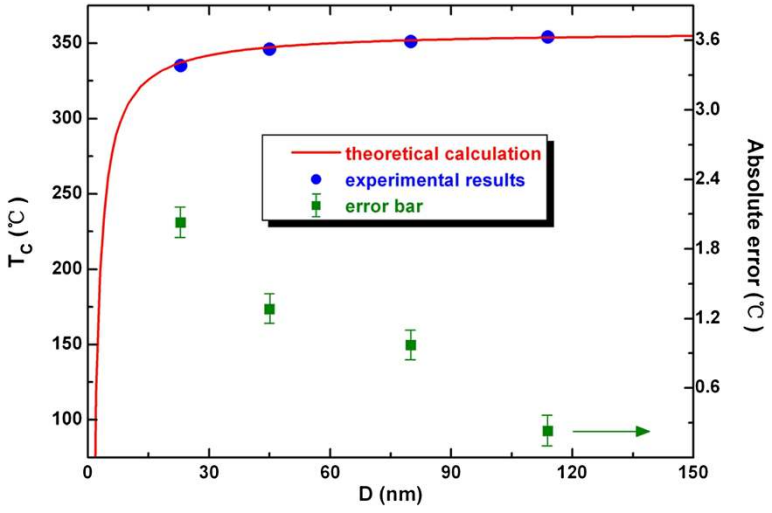

Figure 5 Size dependence of Curie temperature. Based on the TG/DTA experimental results (solid circles) and that of theoretical calculation (red solid line).

temperature T_{Cn} of nanoparticles with both size and shape dependence as

$$T_{Cn} = T_{Cb}\left(1 - \frac{6\mu}{n^{1/3}C^{2/3}\pi k^2}\right), \quad (2)$$

where T_{Cb} is the Curie temperature of the corresponding bulk materials. Further, for spherical nanoparticles, the atomic number n can be expressed as

$$n = \frac{\rho\frac{4}{3}\pi\left(\frac{D}{2}\right)^3}{M}N_A, \quad (3)$$

where ρ is the density of materials, D denotes the particle size of nanoparticles, M is the molar mass of matter, and N_A is the Avogadro constant. Considering our samples of spherical Ni nanoparticles with *fcc* structure, the μ, C, and k are 0.806, 4, and $\sqrt{2}/4$ [35], respectively. Accordingly, substituting the correlative parameters (ρ = 8.908 g/cm^3, M = 58.69 g/mol [36], $N_A = 6.02 \times 10^{23}$ mol^{-1}, T_{Cb} = 358°C [25]) into Equations (2) and (3), the Curie temperature T_C of Ni nanoparticles with particle size D can be expressed as

$$T_C = 358 - 482.38/D. \quad (4)$$

The variation of T_C as a function of particle size calculated using Equation (4) is compared with the TG/DTA results. Specifically, the absolute error between the two results has been given by the error bars in Figure 5, and the obtained relative errors are less than 1%. Through this, we can understand that T_C decreases with decrease of particle size D, and there is a good match between theoretical and experimental results. In other words, the model represents well the size dependence of the Curie temperature of Ni nanoparticles.

Further, the temperature-dependent magnetization was studied by VSM. Figure 6a shows the typical M-T curves of the Ni nanoparticles with various sizes and the corresponding bulk Ni sample. To get the accurate T_C, the M^{-1}-T curves are also given in Figure 6b. According to the Curie-Weiss law, the horizontal axis intercept of M^{-1}-T curve is the Curie temperature T_C of ferromagnetic materials. Therefore, the T_C values are observed to be 337°C, 347°C, 352°C, and 354°C for the Ni nanoparticles with sizes of 23, 45, 80, and 114 nm, respectively. At the same time, the T_C of bulk Ni sample remains 358°C. It goes without saying that the variation trend and the absolute value of T_C confirm the results of TG/DTA measurements.

Nickel is an important magnetic material. To further investigate the magnetic properties of Ni nanoparticles, magnetic measurements of the four Ni-nanoparticle samples with different particle sizes were carried out. Figure 7 shows their room-temperature hysteresis loops. All four samples show hysteresis behavior, revealing that the nanoparticles are ferromagnetic. With increasing particle sizes, the magnetization of the samples increases with applied field. The saturation magnetization M_S for all samples are listed in Table 1. The M_S value of sample *d* determined at room temperature in a field of 1 T is close to that of bulk nickel (M_{Sb} = 54.4 emu/g) [8], indicating the metallic characteristic at this state of Ni nanoparticles. The relatively lower M_S of 40.47 emu/g for sample *a* can be reasonably considered to be due to the smaller particle size as well as to the accompanied increase of specific surface area. The decrease of M_S with decreasing particle size is consistent with that reported previously [37].

Based on the inset of Figure 7, the remanent magnetization M_r and coercivity H_C of all Ni-nanoparticle samples are obtained and also listed in Table 1. As shown in

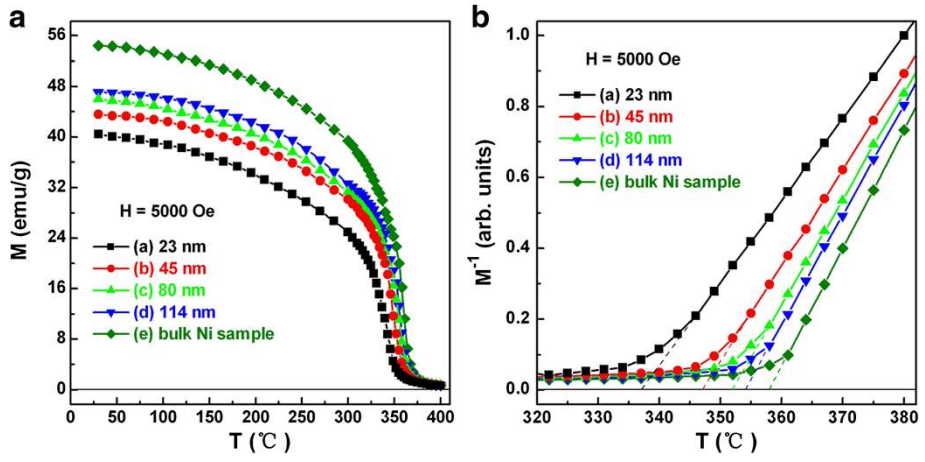

Figure 6 *M*-*T* (a) and M^{-1}-*T* (b) curves. Ni nanoparticles with particle sizes of (a) 23, (b) 45, (c) 80, (d) 114 nm, and (e) the corresponding bulk Ni sample.

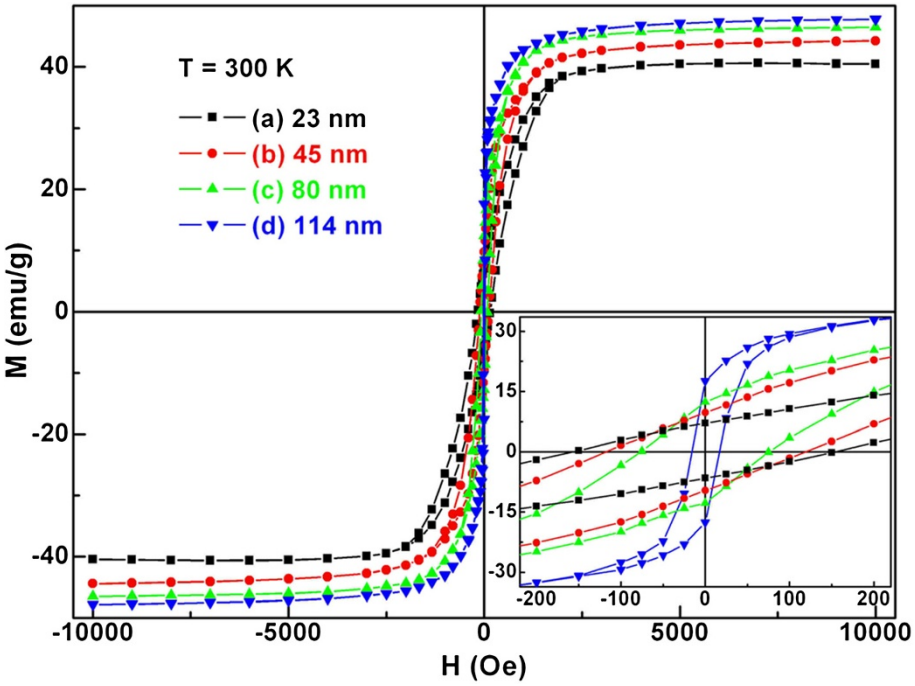

Figure 7 Room-temperature hysteresis loops. Ni nanoparticles with particle sizes of (a) 23, (b) 45, (c) 80, and (d) 114 nm. Inset shows greater detail of the measurements around the origin.

Figure 8, the M_S, M_r, and H_C of spherical Ni nanoparticles are size-dependent. More specifically, the M_S and M_r increase and the H_C decreases monotonously with increasing D, indicating a distinct size effect. According to the effect of particle size on the magnetic coercivity [38], the H_C of the multidomain ferromagnetic nanoparticles conforms to the rule of $H_C \propto 1/D$. However, the single domain size of nickel, 21.2 nm, has been calculated by the magnetic domain theory [37]. Obviously, the particle size for the all current Ni samples is larger than this value. Hence, it is understandable to observe a decline of coercivity with rise of particle size in the case of Ni nanoparticles.

In order to rationalize the decrease of saturation magnetization with decreasing particle size in proportion to the

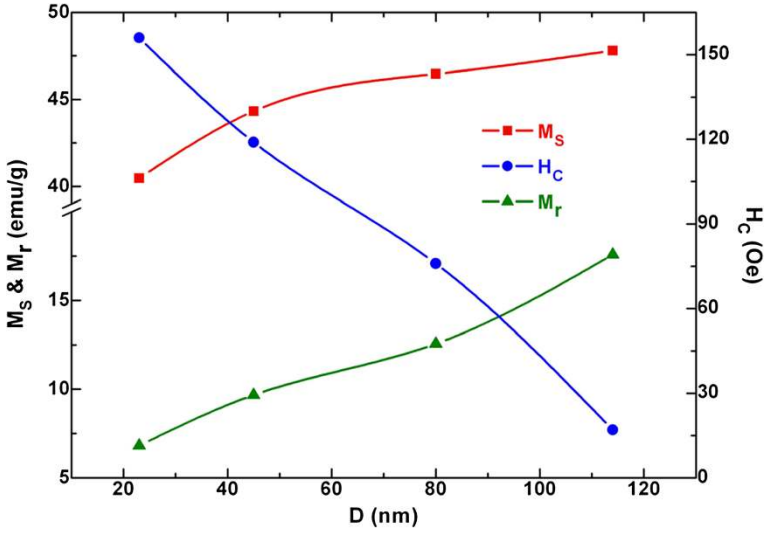

Figure 8 Size dependence of magnetic parameters. Saturation magnetization M_S, remanent magnetization M_r, and coercivity H_C in the case of spherical Ni nanoparticles.

specific surface area of the particles, a magnetically dead layer theory has been developed [39]. In the theory, the saturation magnetization M_{Sn} of nanoparticles follows the formula [40]

$$M_{Sn} = M_{Sb}(1-6t/D), \tag{5}$$

where M_{Sb} denotes the saturation magnetization of the corresponding bulk materials, t is the thickness of magnetically inactive layer, and D is the diameter of nanoparticles. Considering our samples of spherical Ni nanoparticles (M_{Sb} = 54.4 emu/g) [8], the percentage of magnetically inactive layer t/D can be calculated using Equation (5). The t/D values for all samples are listed in Table 1. Clearly, as the surface-to-volume ratio of Ni nanoparticles increases with decreasing particle size, the percentage of magnetically inactive layer increases too. In fact, as the particle size reduced from 114 to 23 nm, the t/D value of Ni nanoparticles slightly increases from 2.03% to 4.26%. This slight change suggests that the dead layer theory cannot satisfactorily explain the size dependence of saturation magnetization [39-41].

Previous studies revealed that the size-dependent effect of saturation magnetization is attributable to the decrease of cohesive energy [42,43]. Generally, the size-dependent cohesive energy E_n of spherical nanoparticles can be described as

$$\frac{E_n}{E_b} = \left(1-\frac{1}{2D/h-1}\right)\exp\left(-\frac{2S_{vib}}{3R}\frac{1}{2D/h-1}\right), \tag{6}$$

where S_{vib} denotes the vibrational part of the overall melting entropy S_m, R is the ideal gas constant, and h denotes the atomic diameter. By incorporating the bond order-length-strength (BOLS) correlation mechanism into the Ising convention and the Brillouin function [44,45], a simplified model can be developed to describe the relationship between the saturation magnetization M_{Sn} of spherical nanoparticles and the average size D of nanoparticles:

$$\frac{M_{Sn}}{M_{Sb}} = 4\left(1-\frac{1}{2D/h-1}\right)\exp\left(-\frac{2S_{vib}}{3R}\frac{1}{2D/h-1}\right)-3. \tag{7}$$

Considering our samples of ferromagnetic Ni nanoparticles, the relevant parameters are M_{Sb} = 54.4 emu/g [8], $S_{vib} \approx S_m$ = 10.12 J mol^{-1} K^{-1} [46], and h = 0.2492 nm [36]. Substituting R = 8.314 J mol^{-1} K^{-1} into Equation (7), the M_S of Ni nanoparticles with size D can be expressed as

$$M_S = 217.6\left(1-\frac{1}{8.0257D-1}\right)\exp\left(\frac{0.8115}{1-8.0257D}\right)-163.2. \tag{8}$$

Shown in Figure 9 is a comparison between the theoretical results based on Equation (8) and the results of VSM measurement. The error bar reveals the difference between the two results, and the maximum value of relative error is 4.52%. Thus, it can be seen that the model prediction is in agreement with the experimental results. In other words, the size-dependent cohesive energy model can describe reasonably well the size dependence of Ni nanoparticles in terms of saturation magnetization. The agreement between the theoretical calculation and experimental results suggests that the drop of M_S is essentially induced by the increase of surface-volume ratio,

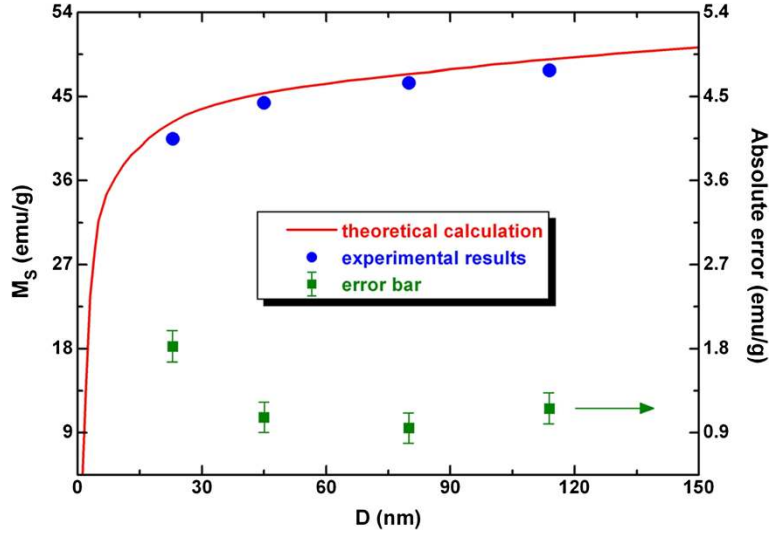

Figure 9 Size dependence of saturation magnetization. For the VSM experimental results (solid circles) and that of theoretical calculation (red solid line).

the same as the size dependence of any thermodynamic amount [47].

Based on the mathematical relation of $\exp(-x) \approx 1 - x$, when x is small enough as a first-order approximation, Equation (7) can be rewritten as

$$\frac{M_{\mathrm{Sn}}}{M_{\mathrm{Sb}}} \approx 1 - \frac{2h}{D}\left(1 + \frac{2S_{\mathrm{vib}}}{3R}\right). \quad (9)$$

Nonetheless, it should be noted that the difference between Equations (7) and (9) becomes evident when the size of nanoparticles further decreases to about several nanometers or smaller scale. Let Equation (9) be equal to zero, namely $M_{\mathrm{Sn}}(D_c) = 0$, where D_c denotes the critical size,

$$D_c \approx 2h[1 + 2S_{\mathrm{vib}}/(3R)]. \quad (10)$$

Substituting the parameters mentioned above into Equation (10), the D_c value of spherical Ni nanoparticles is 0.90 nm. As shown in the final column of Table 1, the percentage of magnetically inactive layer is 4.26%, 3.09%, 2.43%, and 2.03% for spherical Ni nanoparticles with particle sizes of 23, 45, 80, and 114 nm, respectively. Using Equation (5), the corresponding thickness t of magnetically inactive layer is 0.98, 1.39, 1.94, and 2.31 nm for the four Ni-nanoparticle samples. Herein, the critical size (D_c = 0.90 nm) and t values are in the same order of magnitude, but the D_c value is significantly smaller than the four t values. Thus, the size-dependent cohesive energy model under critical condition is consistent with the magnetically dead layer theory.

Conclusions

We systematically studied the size-dependent magnetic properties of spherical Ni nanoparticles in terms of experimental measurement and theoretical calculation. Our results show that the Curie temperature, saturation magnetization, and remanent magnetization increase whereas the coercivity decreases monotonously with the increase of particle size. According to the size-dependent cohesive energy model, a simplified theoretical calculation can be applied to analyze the size dependence of Curie temperature and saturation magnetization. The results of calculation are in good agreement with the experimental results. Under critical condition of critical size D_c = 0.90 nm, the size dependence of magnetization obtained by cohesive energy model is consistent with the analysis of magnetically dead layer theory. With the particle size decreasing, the surface-to-volume ratio of Ni nanoparticles increases and the percentage of magnetically inactive layer increases as well.

Competing interests

The authors declare that they have no competing interests.

Authors' contributions

XH carried out the experiment and prepared the manuscript. WZ participated in the design of the study and helped to draft the manuscript. CA and YD helped in the discussion and analysis of the experimental results. All authors read and approved the final manuscript.

Acknowledgements

The authors greatly acknowledge finical support of the National Natural Science Foundation of China (grant no. 11174132), the National Key Project for Basic Research (grant nos. 2011CB922102 and 2012CB932304), and PAPD, People's Republic of China.

Author details

[1]National Laboratory of Solid State Microstructures and Jiangsu Provincial Laboratory for NanoTechnology, Department of Physics, Nanjing University, Nanjing 210093, China. [2]Department of Chemistry, Hong Kong Baptist University, Hong Kong 852, China.

Received: 13 July 2013 Accepted: 25 September 2013
Published: 28 October 2013

References

1. Feygenson M, Kou A, Kreno LE, Tiano AL, Patete JM, Zhang F, Kim MS, Solovyov V, Wong SS, Aronson MC: **Properties of highly crystalline NiO and Ni nanoparticles prepared by high-temperature oxidation and reduction.** *Phys Rev B* 2010, **81:**014420.
2. Baudouin D, Rodemerck U, Krumeich F, de Mallmann A, Szeto KC, Ménard H, Veyre L, Candy JP, Webb PB, Thieuleux C, Copéret C: **Particle size effect in the low temperature reforming of methane by carbon dioxide on silica-supported Ni nanoparticles.** *J Catal* 2013, **297:**27–34.
3. Khurana JM, Yadav S: **Highly monodispersed PEG-stabilized Ni nanoparticles: proficient catalyst for the synthesis of biologically important spiropyrans.** *Aust J Chem* 2012, **65:**314–319.
4. Bussamara R, Eberhardt D, Feil AF, Migowski P, Wender H, de Moraes DP, Machado G, Papaléo RM, Teixeira SR, Dupont J: **Sputtering deposition of magnetic Ni nanoparticles directly onto an enzyme surface: a novel method to obtain a magnetic biocatalyst.** *Chem Commun* 2013, **49:**1273–1275.
5. Lee KB, Park S, Mirkin CA: **Multicomponent magnetic nanorods for biomolecular separations.** *Angew Chem Int Ed* 2004, **43:**3048–3050.
6. Kalita P, Singh J, Singh MK, Solanki PR, Sumana G, Malhotra BD: **Ring like self assembled Ni nanoparticles based biosensor for food toxin detection.** *Appl Phys Lett* 2012, **100:**093702.
7. Ma F, Huang JJ, Li JG, Li Q: **Microwave properties of sea-urchin-like Ni nanoparticles.** *J Nanosci Nanotechnol* 2009, **9:**3219–3223.
8. Roy A, Srinivas V, Ram S, Chandrasekhar-Rao TV: **The effect of silver coating on magnetic properties of oxygen-stabilized tetragonal Ni nanoparticles prepared by chemical reduction.** *J Phys Condens Matter* 2007, **19:**346220.
9. García-Cerda LA, Bernal-Ramos KM, Montemayor SM, Quevedo-López MA, Betancourt-Galindo R, Bueno-Báques D: **Preparation of *hcp* and *fcc* Ni and Ni/NiO nanoparticles using a citric acid assisted pechini-type method.** *J Nanomater* 2011. doi: 10.1155/2011/162495.
10. Ma F, Ma J, Huang JJ, Li JG: **The shape dependence of magnetic and microwave properties for Ni nanoparticles.** *J Magn Magn Mater* 2012, **324:**205–209.
11. Leng YH, Wang YT, Li XG, Liu T, Takahashhi S: **Controlled synthesis of triangular and hexagonal Ni nanosheets and their size-dependent properties.** *Nanotechnology* 2006, **17:**4834–4839.
12. Chen WM, Zhou W, He L, Chen CP, Guo L: **Surface magnetic states of Ni nanochains modified by using different organic surfactants.** *J Phys Condens Matter* 2010, **22:**126003.
13. Akamaru S, Inoue M, Honda Y, Taguchi A, Abe T: **Preparation of Ni nanoparticles on submicron-sized Al_2O_3 powdery substrate by polyhedral-barrel-sputtering technique and their magnetic properties.** *Jpn J Appl Phys* 2012, **51:**065201.
14. Maicas M, Sanz M, Cui H, Aroca C, Sánchez P: **Magnetic properties and morphology of Ni nanoparticles synthesized in gas phase.** *J Magn Magn Mater* 2010, **322:**3485–3489.
15. Saito G, Hosokai S, Akiyama T, Yoshida S, Yatsu S, Watanabe S: **Size-controlled Ni nanoparticles formation by solution glow discharge.** *J Phys Soc Jpn* 2010, **79:**083501.

16. Calandra P: **Synthesis of Ni nanoparticles by reduction of $NiCl_2$ ionic clusters in the confined space of AOT reversed micelles.** *Mater Lett* 2009, **63:**2416–2418.
17. Gonzalez I, De-Jesus JC, Cañizales E, Delgado B, Urbina C: **Comparison of the surface state of Ni nanoparticles used for methane catalytic decomposition.** *J Phys Chem C* 2012, **116:**21577–21587.
18. Choo S, Lee K, Jo Y, Yoon SM, Choi JY, Kim JY, Park JH, Lee KJ, Lee JH, Jung MH: **Interface effect of magnetic properties in Ni nanoparticles with a *hcp* core and *fcc* shell structure.** *J Nanosci Nanotechnol* 2011, **11:**6126–6130.
19. Kotoulas A, Gjoka M, Simeonidis K, Tsiaoussis I, Angelakeris M, Kalogirou O, Dendrinou-Samara C: **The role of synthetic parameters in the magnetic behavior of relative large *hcp* Ni nanoparticles.** *J Nanopart Res* 2011, **13:**1897–1908.
20. Carroll KJ, Ulises-Reveles J, Shultz MD, Khanna SN, Carpenter EE: **Preparation of elemental Cu and Ni nanoparticles by the polyol method: an experimental and theoretical approach.** *J Phys Chem C* 2011, **115:**2656–2664.
21. Bala T, Gunning RD, Venkatesan M, Godsell JF, Roy S, Ryan KM: **Block copolymer mediated stabilization of sub-5 nm superparamagnetic nickel nanoparticles in an aqueous medium.** *Nanotechnology* 2009, **20:**415603.
22. Yamauchi Y, Itagaki T, Yokoshima T, Kuroda K: **Preparation of Ni nanoparticles between montmorillonite layers utilizing dimethylaminoborane as reducing agent.** *Dalton Trans* 2012, **41:**1210–1215.
23. Mourdikoudis S, Simeonidis K, Vilalta-Clemente A, Tuna F, Tsiaoussis I, Angelakeris M, Dendrinou-Samara C, Kalogirou O: **Controlling the crystal structure of Ni nanoparticles by the use of alkylamines.** *J Magn Magn Mater* 2009, **321:**2723–2728.
24. Bradley JS, Tesche B, Busser W, Maase M, Reetz MT: **Surface spectroscopic study of the stabilization mechanism for shape-selectively synthesized nanostructured transition metal colloids.** *J Am Chem Soc* 2000, **122:**4631–4636.
25. Cullity BD, Graham CD: *Introduction to Magnetic Materials.* Piscataway: IEEE Press; 2009.
26. Gong W, Li H, Zhao ZR, Chen JC: **Ultrafine particles of Fe, Co, and Ni ferromagnetic metals.** *J Appl Phys* 1991, **69:**5119–5121.
27. Tzitzios V, Basina G, Gjoka M, Alexandrakis V, Georgakilas V, Niarchos D, Boukos N, Petridis D: **Chemical synthesis and characterization of *hcp* Ni nanoparticles.** *Nanotechnology* 2006, **17:**3750–3755.
28. Singh V, Srinivas V, Ram S: **Structural and magnetic properties of polymer-stabilized tetragonal Ni nanoparticles.** *Philos Mag* 2010, **90:**1401–1414.
29. Leontyev V: **Magnetic properties of Ni and Ni-Cu nanoparticles.** *Phys Stat Sol (b)* 2013, **250:**103–107.
30. Peng TC, Xiao XH, Wu W, Fan LX, Zhou XD, Ren F, Jiang CZ: **Size control and magnetic properties of single layer monodisperse Ni nanoparticles prepared by magnetron sputtering.** *J Mater Sci* 2012, **47:**508–513.
31. He T, Chen DR, Jiao XL: **Controlled synthesis of Co_3O_4 nanoparticles through oriented aggregation.** *Chem Mater* 2004, **16:**737–743.
32. Morrish AH: *The Physical Principles of Magnetism.* Piscataway: IEEE Press; 2001.
33. Xie D, Wang MP, Cao LF: **A simplified model to calculate the higher surface energy of free-standing nanocrystals.** *Phys Stat Sol (b)* 2005, **242:**R76–R78.
34. Rytkönen A, Valkealahti S, Manninen M: **Melting and evaporation of argon clusters.** *J Chem Phys* 1997, **106:**1888–1892.
35. Askeland DR, Phule PP: *The Science and Engineering of Materials.* New York: Thomson Learning Inc; 2003.
36. *Web elements periodic table.* http://www.webelements.com/nickel/. Accessed 25 March 2013.
37. Shafi KVPM, Gedanken A, Prozorov R, Balogh J: **Sonochemical preparation and size-dependent properties of nanostructured $CoFe_2O_4$ particles.** *Chem Mater* 1998, **10:**3445–3450.
38. Sharifi I, Shokrollahi H, Amiri S: **Ferrite-based magnetic nanofluids used in hyperthermia applications.** *J Magn Magn Mater* 2012, **324:**903–915.
39. Kodama RH: **Magnetic nanoparticles.** *J Magn Magn Mater* 1999, **200:**359–372.
40. Tang ZX, Sorensen CM, Klabunde KJ, Hadjipanayis GC: **Size-dependent Curie temperature in nanoscale $MnFe_2O_4$ particles.** *Phys Rev Lett* 1991, **67:**3602–3605.
41. Yamada O, Ono F, Nakai I, Maruyama H, Ohta K, Suzuki M: **Comparison of magnetic properties of Fe-Pt and Fe-Pd invar alloys with those of Fe-Ni invar alloys.** *J Magn Magn Mater* 1983, **31–34**(1):105–106.
42. Yang CC, Jiang Q: **Size and interface effects on critical temperatures of ferromagnetic, ferroelectric and superconductive nanocrystals.** *Acta Mater* 2005, **53:**3305–3311.
43. Sun CQ, Zhong WH, Li S, Tay BK, Bai HL, Jiang EY: **Coordination imperfection suppressed phase stability of ferromagnetic, ferroelectric, and superconductive nanosolids.** *J Phys Chem B* 2004, **108:**1080–1084.
44. Zhong WH, Sun CQ, Li S: **Size effect on the magnetism of nanocrystalline Ni films at ambient temperature.** *Solid State Commun* 2004, **130:**603–606.
45. Zhong WH, Sun CQ, Li S, Bai HL, Jiang EY: **Impact of bond-order loss on surface and nanosolid magnetism.** *Acta Mater* 2005, **53:**3207–3214.
46. Jiang Q, Zhao DS, Zhao M: **Size-dependent interface energy and related interface stress.** *Acta Mater* 2001, **49:**3143–3147.
47. Jiang Q, Li JC, Chi BQ: **Size-dependent cohesive energy of nanocrystals.** *Chem Phys Lett* 2002, **366:**551–554.

doi:10.1186/1556-276X-8-446
Cite this article as: He *et al.*: Size dependence of the magnetic properties of Ni nanoparticles prepared by thermal decomposition method. *Nanoscale Research Letters* 2013 **8**:446.